

PAPER

The double pendulum: a numerical study

To cite this article: A M Calvão and T J P Penna 2015 *Eur. J. Phys.* **36** 045018

View the [article online](#) for updates and enhancements.

You may also like

- [Cell–substrate interactions](#)
Margaret Gardel and Ulrich Schwarz
- [The Earth radiation balance as driver of the global hydrological cycle](#)
Martin Wild and Beate Liepert
- ['Best article' prize for the 5th anniversary of *Environmental Research Letters*](#)
Dan Kammen and Guillaume Wright

The double pendulum: a numerical study

A M Calvão¹ and T J P Penna^{2,3,4}

¹ Department of Physics, PUC-Rio, Rio de Janeiro, RJ, Brazil

² Instituto de Física, Universidade Federal Fluminense, Niterói, RJ, Brazil

³ Instituto de Ciências Exatas, Universidade Federal Fluminense, Volta Redonda, RJ, Brazil

⁴ National Institute for Complex Systems—CNPq, Brazil

E-mail: thadeupenna@id.uff.br

Received 15 December 2014, revised 10 March 2015

Accepted for publication 17 April 2015

Published 27 May 2015



CrossMark

Abstract

Analysis and characterization of dynamical systems is a common task in computational physics. It frequently demands new algorithms for finding solutions and new techniques for analysing the results. Here we review some of these algorithms and techniques in the study of the double pendulum, which, despite being a very simple mechanical system, can display complex behaviour. Even though it has been studied before (Yu and Bi 1998 *J. Sound Vib.* **217** 691736; Stachowiak and Okada 2006 *Chaos, Solitons & Fractals* **29** 417422; Rafat, Wheatland and Bedding 2009 *Am. J. Phys.* **77** 216–23; Levien and Tan 1993 *Am. J. Phys.* **61** 103844), here we present a deeper discussion of the several methods and algorithms that are used in typical studies of dynamical systems. In addition, we present new results obtained through techniques commonly used in the analysis of complex systems.

Keywords: dynamical systems, chaos, time series

1. Introduction

Introductory courses on numerical methods usually focus on methods rather than the analysis of the system dynamics, using very trivial examples to illustrate the methods. Here we intend to present a numerical study of the double pendulum, a system with a singular and challenging dynamics. Because it is easy to build in practice, the problem can also raise the motivation and stir the curiosity of the students by looking at the beauty of the dynamics of a real double pendulum. The target audience of this article is undergraduate students who had at least a course on classical mechanics and computer programming. The approach described here can be used as a guide for the analysis of other dynamical systems.

Models of dynamical systems displaying complex behaviour are of interest in many areas of science; see [5] for a recent review. Current computational power enables us to simulate

many situations, from molecular dynamics to disease spreading. Those simulations provide information about the system behaviour, allowing for a deeper understanding of it. This analysis has taught us that a collection of simple entities brought together may give rise to new phenomena that are not trivially inferred from their individual behaviours.

The present manuscript is a numerical exploration of the double pendulum focusing on its properties but keeping the implementation of the tools still simple for our target audience. Even though it is a simple system and its equations of motion can be easily obtained using either Newton's laws or the Lagrangian formalism, it is not straightforward to understand or predict its time evolution. One might think that a double pendulum is just the coupling of two simple pendula, and therefore the dynamics of a double pendulum might resemble that of a simple pendulum. However, that is not the case: the double pendulum does exhibit distinct behaviour, e.g., chaos. It is an impressive example that '*More is Different*' [6].

As an additional motivational point, there are many mechanical systems whose behaviour can be understood in terms of double pendula, e.g., mechanical apparatuses such as cranes and robot arms. Even human movements may be modeled by double pendula, as demonstrated in [7] for the golfer swing. The double pendulum is also important in the study of control techniques [8–10].

Frequently, dynamical systems are described by nonlinear differential or difference equations. Analytical solutions for these equations are not available, and approximation methods such as linearization would destroy the complex behaviour of the system, making the analysis useless. Thus, numerical computation in such situations is unavoidable. Therefore, proper attention should be paid to the choice of integration method and its parameters. From a pedagogical point of view, it is one of the most important points raised in this work. Nevertheless, it is not difficult to find studies about dynamical systems that do not go deep in the numerical method used, but rather going straight to the results [1–3, 11, 12]. Because of this we compare methods used by previous papers on the double pendulum, presenting new results and pointing out their pros and cons.

This paper is organized as follows: in section 2, we present a derivation of the equations of motion for the double pendulum using the Lagrangian formalism, which is accessible to undergraduate students. In section 3, we present the numerical methods we employed to solve the equations of motion. We discuss their validity in order to determine the range of parameters for which the solutions are reliable. We also discuss the computational effort needed for each method. In section 4, we present the main results obtained with the methods discussed in the previous section. The first one is the characteristic Lyapunov exponent, which is a measure of how chaotic the system is. Surprisingly, despite the importance of the double pendulum and its use as a paradigm of a chaotic system, there is not, to the best of our knowledge, any extensive study of its Lyapunov exponent. Because its relation with chaos is direct, we chose to work with its numerical analysis—although it is not one of easy implementation. That is why we decide to present alternative schemes, allowing a qualitative analysis and even a quantitative one when it is possible without raising the difficulty level of implementations. The second method is the bifurcation diagram, also widely used to characterize chaos. After the presentation of those classical methods of chaos theory, we characterize the double pendulum time series using linear methods, represented by the Fourier analysis and the autocorrelation function. Time series analysis is important when performing an experiment, since it is the one thing at our disposal. Thus, it is helpful to understand how methods of time series analysis behave on a known system. A comparison between these methods is then presented. Furthermore, we will comment on the recurrence plots, a nonlinear method that has been shown to provide very good results on dynamical system analysis.

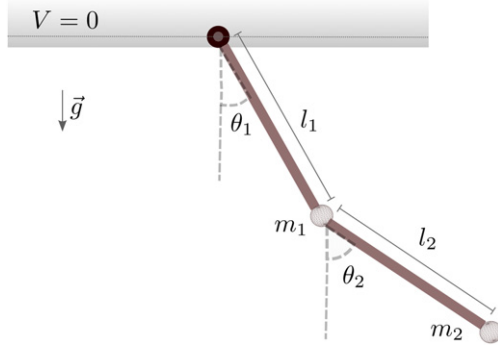


Figure 1. A schematic double pendulum. We choose the pivot of the first rod as the origin of the coordinate system and its level as reference for the gravitational potential, i.e., $V = 0$. The pendula are hanging straight down for $\theta_1 = \theta_2 = 0$.

Finally, we present the trajectories of the pendulum masses, which will be compared to other results, and our conclusions.

2. Mathematical model

The purpose of this section is to introduce the double pendulum problem and to find its equations of motion. Using the coordinate system presented in figure 1, one can write the following Lagrangian [13]:

$$\mathcal{L} = m_2 l_1 \omega_1 l_2 \omega_2 \cos(\theta_1 - \theta_2) + g l_1 (m_1 + m_2) \cos(\theta_1) + g m_2 l_2 \cos(\theta_2) \quad (1)$$

$$+ \frac{1}{2} l_1^2 (m_1 + m_2) \omega_1^2 + \frac{1}{2} m_2 l_2^2 \omega_2^2 \quad (2)$$

where l_1, l_2 are the length of the massless rods, m_1, m_2 are the masses of each pendulum and $\omega_1 = \dot{\theta}_1$, $\omega_2 = \dot{\theta}_2$.

From the Euler–Lagrange equations,

$$\frac{d}{dt} \frac{\partial \mathcal{L}}{\partial \dot{\theta}_1} - \frac{\partial \mathcal{L}}{\partial \theta_1} = 0 \quad (3a)$$

$$\frac{d}{dt} \frac{\partial \mathcal{L}}{\partial \dot{\theta}_2} - \frac{\partial \mathcal{L}}{\partial \theta_2} = 0, \quad (3b)$$

we can find

$$0 = l_1 \left[(m_1 + m_2) (g \sin(\theta_1) + l_1 \dot{\theta}_1) + l_2 m_2 \omega_2^2 \sin(\theta_1 - \theta_2) + m_2 l_2 \dot{\theta}_2 \cos(\theta_1 - \theta_2) \right] \quad (4a)$$

$$0 = m_2 l_2 \left[g \sin(\theta_2) + l_2 \dot{\theta}_2 - l_1 \omega_1^2 \sin(\theta_1 - \theta_2) + l_1 \dot{\theta}_1 \cos(\theta_1 - \theta_2) \right]. \quad (4b)$$

The limit cases of the double pendulum equations can be found. Setting one parameter to zero while keeping the others from vanishing in equation (4) leads to the conclusion:

1. $l_1 = 0$ makes (4a) vanish, and (4b) is now the equation for a simple pendulum of length l_2 and mass m_2 .
2. $l_2 = 0$, makes (4b) vanish, and (4a) is now the equation for a simple pendulum of length l_1 and mass m_1 .
3. $m_2 = 0$, makes (4b) vanish, and (4a) also leads to a simple pendulum of length l_1 and mass m_1 .

These limit cases can be interesting for testing the implementation of numerical methods. Introducing a dimensionless parameter $\Gamma \equiv m_1/m_2$ on equation (4) leads to

$$0 = l_1 [(\Gamma + 1)(g \sin(\theta_1) + l_1 \dot{\theta}_1) + l_2 \omega_2^2 \sin(\theta_1 - \theta_2) + l_2 \dot{\theta}_2 \cos(\theta_1 - \theta_2)] \quad (5a)$$

$$0 = l_2 [g \sin(\theta_2) + l_2 \dot{\theta}_2 - l_1 \omega_1^2 \sin(\theta_1 - \theta_2) + l_1 \dot{\theta}_1 \cos(\theta_1 - \theta_2)]. \quad (5b)$$

This means that the number of parameters that control the dynamics of the system can be reduced to three: two lengths l_1 , l_2 and the ratio Γ between the masses m_1 , m_2 .

3. Numerical analysis

We will present here the Runge–Kutta, the Adams–Bashforth and the Adams–Moulton methods [14, 15]. Before discussing each numerical method, it is important to perform a physical analysis of the problem to find features that could make the numerical solution an easier task.

For dynamical systems, it is interesting to look for symmetries or, in other words, conserved quantities [13]. They are crucial to test results. While some dynamical variables can change in an unpredictable manner, conserved quantities do not, although they can be complicated functions of the system variables. Therefore, it is advisable to check if known conserved quantities are in fact constants of motion (within a given tolerance) in the numerical solutions.

For the double pendulum without friction, the obvious conserved quantity is the mechanical energy. On a numerical integration, there are fluctuations on the conserved quantity related to the numerical error. To express how large the fluctuations are, a reference energy, E_{ref} , must be defined. The energy of the standing up configuration at rest is a good choice; it corresponds to the maximum value for the potential energy, and figure 2(b) illustrates it. Since we will only consider the pendulum released from rest, $\omega_1(0) = \omega_2(0) = 0$, E_{ref} will also be the maximum value of the mechanical energy. With these definitions, it is expected that the energy fluctuations will be much smaller than E_{ref} for a good numerical method.

In this section we are considering $\theta_1(0) = \theta_2(0)$ in all initial conditions. The pendulum is then left to fall at different heights as illustrated in figure 2(a). Therefore, the pendulum will always have an energy smaller than E_{ref} .

From now on, we discuss each numerical method in detail, using the following values for the parameters: $m_1 = m_2 = 0.1$ kg, $l_1 = l_2 = 0.3$ m and $g = 9.8$ m s⁻².

3.1. Fourth-order Runge–Kutta method

The classical Euler and the improved Euler are the most basic numeric methods for solving dynamical equations. They can be combined to create better methods such as the well-known Runge–Kutta methods. These are relatively easy to implement and the fourth-order method is precise enough to handle many problems efficiently.

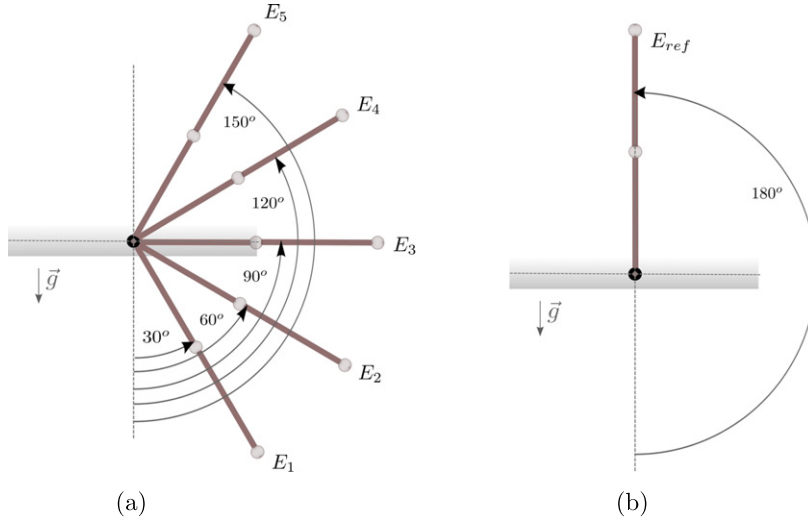


Figure 2. All the numerical tests are conducted with the initial conditions illustrated in figure 2(a); the pendulum is left to a free fall, $\omega_1(0) = \omega_2(0) = 0$, from those angles, $30^\circ, 60^\circ, 90^\circ, 120^\circ, 150^\circ$. The pendulum position of the reference energy chosen is illustrated in figure 2(b), $\omega_1(0) = \omega_2(0) = 0$ and $\theta_1(0) = \theta_2(0) = 0$. (a) Different initial conditions considered ($\theta_1(0) = \theta_2(0)$). (b) Position of the pendulum used for the reference energy E_{ref} .

To solve the equation

$$\frac{d\vec{x}}{dt} = \vec{f}(t, \vec{x}), \vec{x}(t_0) = \vec{x}_0. \quad (6)$$

the fourth-order Runge–Kutta prescribes

$$\vec{x}_{n+1} = \vec{x}_n + \delta t \left(\frac{\vec{k}_{1,n} + 2\vec{k}_{2,n} + 2\vec{k}_{3,n} + \vec{k}_{4,n}}{6} \right) \quad (7)$$

where

$$\begin{aligned} \vec{k}_{1,n} &= \vec{f}\left(t_n, \vec{x}_n\right) \\ \vec{k}_{2,n} &= \vec{f}\left(t_n + \frac{1}{2}\delta t, \vec{x}_n + \frac{1}{2}\delta t \vec{k}_{1,n}\right) \\ \vec{k}_{3,n} &= \vec{f}\left(t_n + \frac{1}{2}\delta t, \vec{x}_n + \frac{1}{2}\delta t \vec{k}_{2,n}\right) \\ \vec{k}_{4,n} &= \vec{f}\left(t_n + \delta t, \vec{x}_n + \delta t \vec{k}_{3,n}\right). \end{aligned} \quad (8)$$

Note that the sum $(\vec{k}_{1,n} + 2\vec{k}_{2,n} + 2\vec{k}_{3,n} + \vec{k}_{4,n})/6$ is the average of the x_n variation on different positions of the interval δt for each dimension n of the system.

This method has a local truncation error proportional to $(\delta t)^4$ and the global error proportional to $(\delta t)^5$ (for a formal derivation see [16]). For this reason it is called the fourth-order method, and it is so by construction.

We included the Runge–Kutta method because it is simple and appears frequently in numerical analysis books [14, 15] and in software packages. It is so common that it may be

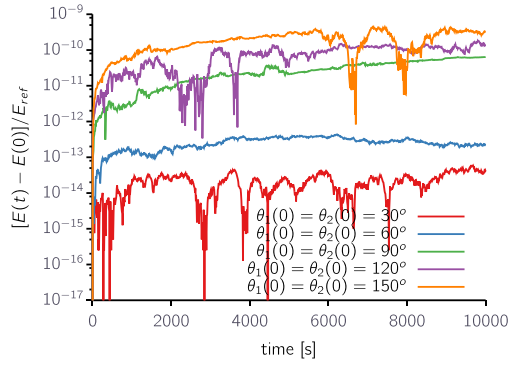


Figure 3. Fluctuation of the energy as a function of the time for different initial conditions. The Runge–Kutta method was used to integrate the equations of motion.

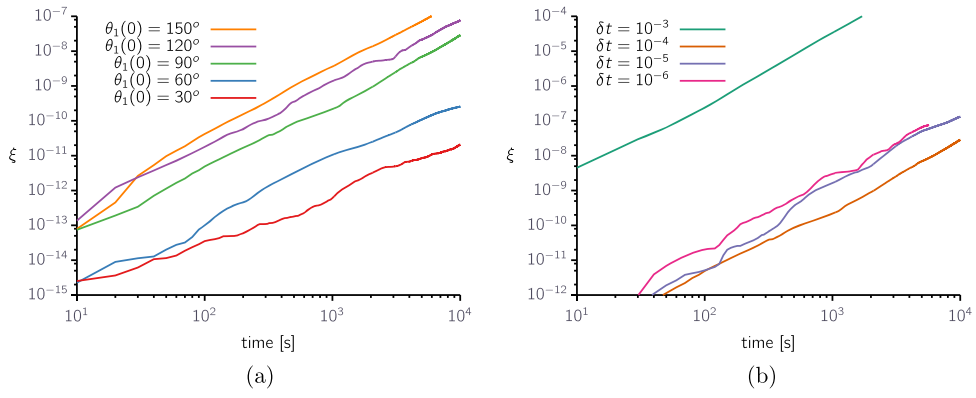


Figure 4. These graphics show the cumulative numerical error, $\xi(t)$, for the Runge–Kutta method on the double pendulum integration. Note that the integration does not necessarily improve with a smaller step, as one would expect. (a) Cumulative error on the energy for different initial conditions ($\delta t = 10^{-4}$, $\theta_2(0) = \theta_1(0)$, $\omega_1(0) = \omega_2(0) = 0$). (b) Cumulative error on the energy for different time steps ($\theta_1(0) = \theta_2(0) = 90^\circ$, $\omega_1(0) = \omega_2(0) = 0$).

considered one of the main tools for the analysis of dynamical systems [1, 3, 12], although sometimes it is used rather blindly. It can also be used as a starting point for other numerical methods, namely the multistep ones, that will also be analysed here.

Back to the double pendulum problem, we can integrate the system equations for $\theta_1(t)$, $\theta_2(t)$, $\omega_1(t)$, $\omega_2(t)$ to obtain the time evolution of the mechanical energy. For a fair comparison, we show in figure 3 the ratio between the variation of the energy, $E(t) - E(0)$, and the reference value E_{ref} . It evidently depends on the initial condition. For a higher angle, there will be bigger fluctuation. A different initial conditions with the same energy will also lead to different results.

Since figure 3 has many fluctuations, it is more convenient to investigate the total cumulative error, $\xi(t) = \sum'_{\mu=t_0}^t \frac{|E(\mu) - E(0)|}{|E_{\text{ref}}|}$, that is a smoother curve easier to interpret. Figure 4(a) shows how the cumulative error depends on the initial condition $\theta_1(0)$. Again, the higher $\theta_1(0)$, the higher the relative error. As the angles grow, and so does the mechanical

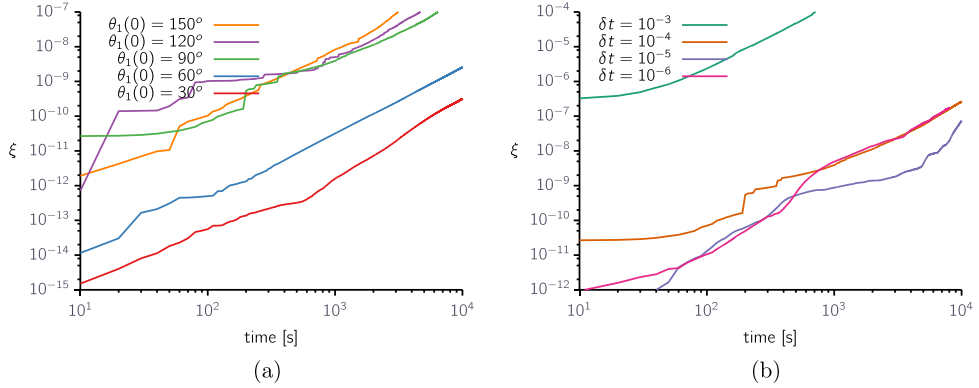


Figure 5. These graphics show the cumulative numerical error, $\xi(t)$, for the Adams–Bashforth method on the double pendulum integration. Note that the integration does not necessarily improve with a smaller step, as one would expect. (a) Cumulative error on the energy for different initial conditions ($\delta t = 10^{-4}$, $\theta_2(0) = \theta_1(0)$, $\omega_1(0) = \omega_2(0) = 0$). (b) Cumulative error on the energy for different time steps ($\theta_1(0) = \theta_2(0) = 90^\circ$, $\omega_1(0) = \omega_2(0) = 0$).

energy, the nonlinear terms get more significant, yielding a more complex trajectory and demanding a greater accuracy of integration to keep the fluctuations under control.

It is usually assumed that a smaller time step (δt) will lead to smaller integration errors. We decided to test this assumption. Figure 4(b) shows the integration results for different δt . Our results indicate that the choicest time step is close to $\delta t = 10^{-4}$. Smaller δt results in smaller precision and higher computing times. This is counterintuitive because, in principle, the Taylor formula is exact in the limit $\delta t \rightarrow 0$. However, besides the mathematical error in the Taylor formula due to a finite δt , there are numerical errors due to the way computers store real numbers with a finite number of decimal digits (the so-called truncation errors). For very small δt these truncation errors become more important than the mathematical error, thus the finite optimal value for δt .

3.2. Fourth-order Adams–Bashforth method

The differential equation (6) can be written as

$$\vec{\phi}(t_{n+1}) - \vec{\phi}(t_n) = \int_{t_n}^{t_{n+1}} \vec{\phi}'(t) dt \quad (9)$$

where $\vec{\phi}$ is the solution of equation (6). The main idea behind the Adams–Bashforth method is to approximate $\vec{\phi}'$ by a polynomial and use it to evaluate the integral at the right side of equation (9). The coefficients of this polynomial can be written as a function of some time steps that can be calculated with a previous method. Using a polynomial of degree three, one can obtain the fourth order Adams–Bashforth formula,

$$\vec{x}_{n+1} = \vec{x}_n + (\delta t / 24) (55\vec{f}_n - 59\vec{f}_{n-1} + 37\vec{f}_{n-2} - 9\vec{f}_{n-3}). \quad (10)$$

Since a polynomial of degree three is used, after the integration, the terms discarded are of the order of δt^4 , and the local truncation error is of this order. Since this equation has a local truncation error of the same order of the fourth-order Runge–Kutta method, it is possible to use the Runge–Kutta method to generate the first steps of the integration needed by the

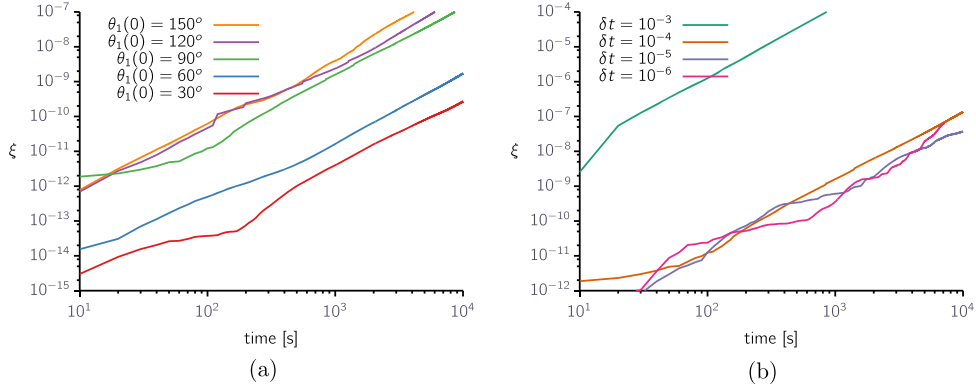


Figure 6. These graphics show the cumulative numerical error, $\xi(t)$, for the Adams–Bashforth method on the double pendulum integration. Note that the integration does not necessarily improve with a smaller step, as one would expect. (a) Cumulative error on the energy for different initial conditions ($\delta t = 10^{-4}$, $\theta_2(0) = \theta_1(0)$, $\omega_1(0) = \omega_2(0) = 0$). (b) Cumulative error on the energy for different time steps ($\theta_1(0) = \theta_2(0) = 90^\circ$, $\omega_1(0) = \omega_2(0) = 0$).

Adams–Bashforth method. From figure 5 it is clear that the Adams–Bashforth method does not perform better than the Runge–Kutta method. It is better to use Runge–Kutta with $\delta t = 10^{-4}$ than Adams–Bashforth with $\delta t = 10^{-5}$. However, comparing the graph at the right of figures 5 and 4, it is clear that the Adams–Bashforth method is less susceptible to changes in the initial conditions. In addition, the Adams–Bashforth method is faster, because the Runge–Kutta method needs four evaluations of the system functions, while Adams–Bashforth needs only one, since we can reuse the previously calculated values for the quantities. Thus, this method appears as a good alternative to the fourth-order Runge–Kutta.

3.3. Fourth-order Adams–Moulton method

This method is just a variation of the Adams–Bashforth and its deduction and implementation are similar:

$$\vec{x}_{n+1} = \vec{x}_n + (\delta t / 24) (9\vec{f}_{n+1} + 19\vec{f}_n - 5\vec{f}_{n-1} + \vec{f}_{n-2}). \quad (11)$$

Because \vec{x}_{n+1} appears on both sides of the equation, as can be seen in equation (11), this method is called ‘implicit.’ It can be shown that this method has a better precision than Adams–Bashforth of the same order [15] and it can be used to correct values from Adams–Bashforth. That is why it is called a predictor-corrector method. This method can also be used to build a variable step method, where the size of the time step is decreased as the corrected value gets much different than the predicted value. Figure 6 shows how this correction performed on the previous result, figure 5. The performance of the Adams–Moulton method can be considered very good, since the error does not change much for different values of δt and the dependence on initial conditions is not worse than for the other two methods presented here. As a side effect it takes twice the time as the Adams–Bashforth method but it is still faster than the Runge–Kutta method.

3.4. Symplectic methods

The methods discussed until now have good local precision; however, they do not preserve important properties of conservative Hamiltonian systems. Thus, it is important to search for numerical methods that preserve these properties, at least, on average. These methods are known as symplectic, and the Hamiltonian formalism is mandatory, where the position and momentum are switched by a set of canonical coordinates, (\mathbf{q}, \mathbf{p}) . The system dynamics are obtained from the Hamiltonian \mathcal{H} , a Legendre transform of the Lagrangian.

There are different symplectic methods, the most common being the explicit ones. There is a strong limitation on their use: the Hamiltonian must be separable, i.e., of the form $\mathcal{H} = T(\mathbf{p}) + V(\mathbf{q})$. We refer the reader to [17], where some the applications of symplectic methods to simple Hamiltonians are presented, and to [18] for a more recent work with adaptive time steps.

The double pendulum has the Hamiltonian

$$\begin{aligned} \mathcal{H} = & \left[-2l_1^2 m_2^2 l_2^2 \left(l_1(m_1 + m_2) \cos(q_1) + \cos(q_2) m_2 l_2 \right) g \left(\cos(-q_2 + q_1) \right)^2 \right. \\ & - 2p_1 l_2 l_1 p_2 m_2 \cos(-q_2 + q_1) + 2g l_1^3 l_2^2 m_2 (m_1 + m_2)^2 \cos(q_1) \\ & \left. + 2g l_2^3 l_1^2 m_2^2 \left(m_1 + m_2 \right) \cos(q_2) + \left(p_1^2 l_2^2 + l_1^2 p_2^2 \right) m_2 + l_1^2 p_2^2 m_1 \right] \\ & / \left[2 \left(-m_1 - m_2 + m_2 \cos^2(-q_2 + q_1) \right) m_2 L_2^2 l_1^2 \right] \end{aligned}$$

that is not separable. Therefore, explicit symplectic methods cannot be used. For a non-separable Hamiltonian there are two options: the generating function and the symplectic version of the Runge–Kutta method.

The generating function method does not have a general implementation. The process to obtain the equations to be integrated involves the manipulation of many different derivatives of the Hamiltonian [19], and for higher orders it is usually a hard task [20].

The symplectic version of the Runge–Kutta methods leads to a system of coupled nonlinear equations that has to be solved at every step using, e.g., the Newton–Raphson method. The convergence is slow, being linear in many cases. Because it demands many function evaluations, the algorithm is usually time consuming. For its implementation details and methods, the interested reader should check [21]. For the double pendulum system in particular, there is a further complication due to its governing equations being quite convoluted and thus its running should be overly slow.

Symplectic methods are commonly used in celestial mechanics (e.g., a planetary system), where many iterations are needed for long-term investigations [22]. In the next sections, the analysis that demands a longer orbit integration is the Lyapunov exponent, but even if it converges on an interval where the energy growth is negligible. Therefore the fact that we are not using a symplectic method for the double pendulum is of no concern, and simpler and faster numerical methods can be used. However, we must be aware of symplectic methods for the analysis of other systems since they might be the only reasonable choice.

3.5. Discussion

If the system equations to be integrated have no conserved quantities, it is important to compare the dynamics generated by some different numerical methods to see if the results are consistent. For conservative systems, a symplectic method may be an option. For a separable

Hamiltonian, simple and explicit symplectic methods can be used; for a non-separable Hamiltonian, these methods are computationally expensive and of hard implementation.

Considering the double pendulum equations, the results presented in this section suggest that the three methods studied have good performances when an appropriate choice of the integration step is made. Even very intricate equations, as the ones governing the double pendulum, can be properly addressed by those simple methods. However, depending on the speed and precision needed, one should be more careful when addressing the numerical integration for larger times.

If computer time is not an issue, then one can choose the Adams–Moulton with a time step between 10^{-4} and 10^{-6} for the standard double precision real number representation. If computation time is at stake, the best method is the Adams–Bashforth. In this case, however, one must pay more attention to the choice of integration step. The Runge–Kutta method also has a decent performance, but it is more sensitive to initial conditions and the step choice than the other methods.

To finalize this section we would like to point out some of our most relevant observations:

- Decreasing the integration step size δt does not always improve integration.
- Different methods may have their own optimum time step sizes.
- The accuracy of each method we have tested strongly depends on the different initial conditions for a nonlinear system.
- An implicit numerical method is useful to minimize the error and to improve the stability, because they usually are more accurate than the explicit ones and they are more robust, for example, concerning the dependence on the time step and the initial conditions.

4. Dynamical analysis

In the last section we discussed how to get reliable numerical results for the dynamics of the double pendulum. Now we proceed to extract useful information from the numerical solution of the system's equations of motion.

The double pendulum has two arms that reminds one of two coupled harmonic oscillators, at least for small energies. From the theory of coupled harmonic oscillators, this can lead to two kinds of dynamics: periodic or quasiperiodic. A periodic motion can only be achieved when the frequencies of the coupled oscillators are commensurable, that is, any of the oscillator frequencies can be expressed as a linear combination of the others. Even though quasiperiodic signals have no characteristic period, it is possible to find one interval that is virtually identical to its adjacent, but not necessarily similar to intervals much farther away in time. These similar intervals are a kind of ‘period’. From now on we will use the term quasiperiodic motion to refer to both dynamics, since periodic motion is a particular case.

In nonlinear systems, the dynamics may go beyond the quasiperiodic motion, exhibiting a very complex behaviour known as chaos. A traditional way to characterize a chaotic system is through its Lyapunov exponents. Although previous studies have evaluated the Lyapunov spectra of the double pendulum for very specific conditions [2, 4], we present here a more extensive study of this quantity. We will also present an analysis in terms of bifurcation diagrams appropriate for recognizing the route to chaos. Then we will analyse the double pendulum time series. This is important. Nonlinear models can generate complex behaviour; once this behaviour is characterized, it is important to understand how it affects the system time series. This knowledge is helpful in the time series analysis of any nonlinear experiment.

We employ the Fourier transforms, a ubiquitous method in the analysis of time series, commonly applied to find the characteristic frequencies or their distribution, and the auto-correlation function that is also common in the literature. Finally, we discuss recurrence plots, which, to the best of our knowledge, have not been discussed previously for the double pendulum. This is a versatile tool that can take into account both the attractor and the time series analysis.

We are going to consider the pendulum released from different angles, as shown in figure 2(a), for both symmetric $\theta_1(0) = \theta_2(0) = \{0, \pi\}$ and asymmetric $\theta_1(0) = \{0, \pi\}$, $\theta_2(0) = 0$ cases. For the reasons discussed in the previous section, we chose to work with the fourth-order Adams–Bashforth method with $\delta t = 10^{-5}$ s. Our choice for the system’s physical parameters were arbitrarily chosen as $m_1 = m_2 = 0.1$ kg, $l_1 = l_2 = 0.3$ m and $g = 9.8$ m s⁻².

4.1. Lyapunov analysis

The phase space is a useful concept to analyse dynamical systems. Each coordinate—and its respective momentum—corresponds to one dimension in the phase space. A point in phase space represents a state, characterized by the set of all positions and momenta, of the system at a specific time. The system’s dynamical evolution will generate an orbit in phase space that contains all the information about the system dynamics for a given initial condition and set of parameters.

If the system is chaotic, then nearby orbits on the phase space will diverge from each other exponentially, i.e., as $e^{\lambda t}$. The exponent λ is called the Lyapunov exponent. The number of these exponents coincides with the dimension of the phase space, and if any of them is positive, the system is said to be chaotic. This behaviour implies sensitive dependence on the initial conditions, which is the main characteristic of chaotic systems.

Lyapunov exponents are defined as

$$\lambda_i = \lim_{t \rightarrow \infty} \lim_{\epsilon_i(t_0) \rightarrow 0} \frac{1}{t} \log_2 \frac{\epsilon_i(t)}{\epsilon_i(t_0)}, \quad i = 1, \dots, m. \quad (12)$$

where m is the phase space dimension, $\epsilon_i(t_0)$ is the initial separation between a test orbit and a reference orbit at t_0 and $\epsilon_i(t)$ is the separation at time t on the dimension i . However, in practice, this is not a very useful definition to calculate the exponent, since, in general, there are no analytical solutions available for nonlinear systems. Nevertheless, there are some proposals on algorithms to estimate the exponent [23–25].

A naive Lyapunov exponent estimation is to use a numerical method to integrate two very close trajectories, and then calculate how the orbits diverge from each other. In practical terms, this method is not appropriate; the divergence will grow exponentially and the finite precision of computer digits would lead to a wrong estimate of the exponent. To circumvent this problem, one can follow the procedure in figure 7, where, after a time τ , another very close orbit is chosen in the same direction of the preceding orbit, and the Lyapunov exponent will be estimated from the mean divergence from many orbits chosen to be very close to the reference orbit. Even though the previous idea seems to be a better recipe, there is still an issue: it is not clear how to choose nearby trajectories.

In fact, there is no need to use more than one orbit on the calculation; one can use the linearized equations, i.e., the Jacobian of the equations of motion (equation (4)). The set of linearized equations describes the behaviour of the system on the neighborhood of a point, allowing an estimate of how nearby trajectories behave. To accomplish this, an orthonormal base must be used as the initial condition of the linearized equations, and a point of the

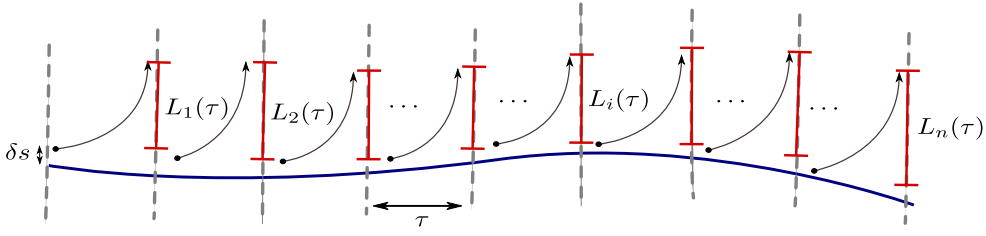


Figure 7. Naive procedure for Lyapunov exponent calculation: get a reference orbit (blue line), choose a point very close to this orbit (black point), now calculate the log of these orbit divergences after a time τ , and repeat the process many times. The logarithm of the divergences, when $\tau \rightarrow 0$ and $\delta s \rightarrow 0$ for a long enough reference orbit, will give an estimate for the largest Lyapunov exponent, $\lambda_{\max} \approx \frac{1}{n} \sum_{j=1}^n \log_2(L_j(\tau)/\delta s)$. For exponential divergence, as represented in this figure, the orbit is considered chaotic.

reference orbit is used to set the linearized equations' parameters. With a numerical integration of the orthonormal base, one can estimate the divergence of the nearby orbits from the changes of the vector sizes. At each iteration, the vectors must be normalized again, enabling an estimation of the growth on the next iteration. This procedure leads to another issue: the base tends to collapse in the direction of greater growth. In order to solve this, a Gram–Schmidt orthonormalization process is also used, enabling an estimation of the Lyapunov exponent on all the directions (see [24] for a FORTRAN code example). The procedure can then be summarized as follows [26]:

1. Initialize the variables of the system of m differential equations. Define m vectors that are initially orthonormal, $\hat{\phi}_i$.
2. Integrate the system to generate a new point of the reference orbit. Use the new reference orbit point on the linearized equations and integrate it to obtain m new vectors, $\vec{\phi}'_i$.
3. Use the orthonormalization process to obtain a new orthonormal basis, $\hat{\phi}''_i$, taking care to hold the vector lengths, $|\vec{\phi}'_i|$, on an array.
4. Accumulate on an array, sum[m], the quantities $l_i(t) = \log_2(|\vec{\phi}'_i|)$, $i = 1, 2, \dots, m$, that is, do $\text{sum}[i] = \text{sum}[i] + l_i(t)$ on every τ step.
5. Print $\text{sum}[i]/t$, that estimates the Lyapunov exponent λ_i at time t .
6. Repeat the steps 2 → 6 until the desired tolerance is achieved.

We can get as many Lyapunov exponents as the dimension of the phase space. This set is called the Lyapunov spectrum. However, an exponent cannot be directly associated with a specific direction or variable.

Autonomous Hamiltonian systems are those that do not depend explicitly on time. Those systems have some symmetries on the Lyapunov spectrum [23]. An important one is that exponents should come in pairs with opposite signs, and at least two of them must be zero. These symmetries can be used as tests; as shown in figure 8(a) our results are in agreement with it. In addition, we found that the estimates of the Lyapunov exponent fluctuate, as is shown in the inset. It is also important to highlight that the convergence of the Lyapunov exponents is obtained on the interval where the integration is reliable; in other words, the energy fluctuations are negligible (see figure 5).

Although the symmetries imply that the interesting quantity for characterizing chaos is the largest Lyapunov exponent λ_{\max} , it is still useful to calculate the whole spectrum of

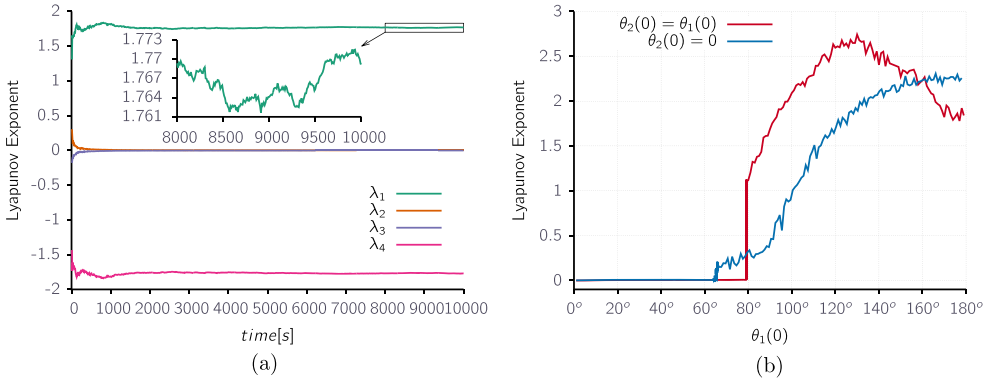


Figure 8. Lyapunov exponents for the double pendulum. In (a) one can see the time evolution for four exponents and how they obey the symmetry requirements. The inset shows the fluctuations of the largest exponent even at large times. In (b) it is shown how the largest Lyapunov exponent depends on the initial conditions for the symmetric and the asymmetric cases. (a) Lyapunov spectrum ($\theta_2(0) = \theta_1(0) = 90^\circ$). (b) The largest Lyapunov exponent (λ_{\max}).

exponents. Because of the fluctuations displayed even at large times, it is tricky to find how long to wait for the Lyapunov calculation to converge. Monitoring the exponents that we know are going to zero, as seen in figure 8(a), could be a way to find this time. There is a clear compromise in this case, though: if we wait too long for the convergence, the numerical methods start to accumulate many errors, as we have shown before.

Figure 8(b) shows that there is a critical angle where the pendulum starts to behave in a chaotic manner. It also makes clear that the initial condition of the pendulum influences when the behaviour changes. The same calculation for the Lyapunov exponent can be found on [4], with a different initial condition, and their results are in good agreement with the ones from figures 8(a) and (b). It is also possible to find one value for the Lyapunov exponent on [2], where they used a different procedure, estimated from the time series [24].

Knowing the system dynamics it is possible to better understand why the numerical method's performance changes with the initial conditions. Note that on figures 4(a), 5(a) and 6(a), the chaotic trajectories have a consistent higher cumulative error. This is a sign that a chaotic trajectory that is more complex is harder to integrate.

In this study we are dealing with an ideal double pendulum, with no friction in its joints. A real double pendulum that is not forced cannot be strictly chaotic. Because of inherent friction, it has a stable fixed point that eventually will attract all the orbits, *viz.*, all the initial conditions end in the same stable configuration $\theta_1(t) = \theta_2(t) = 0$ for a long enough time. This implies a negative Lyapunov exponent, since orbits from different initial conditions end in the same fixed point, getting closer among themselves. However, for the cases of small dissipation and/or for short time interval of observation, one may neglect the friction and the orbit should resemble the one from a conservative system. This should, in principle, imply that the motion of a real double pendulum resemble the one of the artificial conservative model, thus justifying the present analysis. The double pendulum has been experimentally studied and can be found in [4, 27].

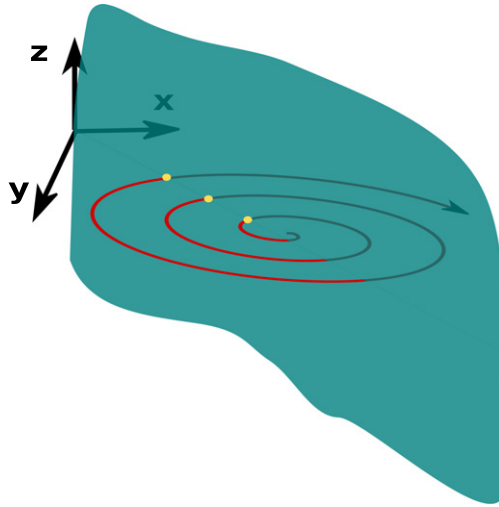


Figure 9. Illustration of a Poincaré section, an interesting qualitative tool to visualize orbits on the phase space. Through a surface (green plane), one records points where the system trajectory crosses it (yellow dots). Rigorously, a surface side is chosen, and only the points that are generated by the trajectory coming from that side are chosen. This better identifies when the system returns to the same state.

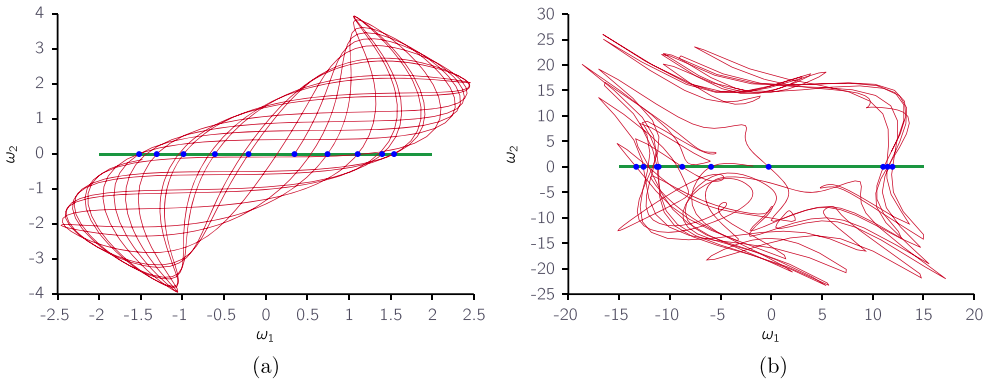


Figure 10. Illustration of an orbit of the double pendulum on a phase plane, red line, and a Poincaré section, green line at $\omega_2 = 0$. The blue dots are the locations where the orbit crosses the Poincaré section. (a) Quasiperiodic motion ($\theta_1(0) = \theta_2(0) = 30^\circ$). (b) Chaotic motion ($\theta_1(0) = \theta_2(0) = 150^\circ$).

4.2. Bifurcation diagrams

Orbits in the phase space—as discussed in section 4.1—are valuable tools to access the system behaviour. However, for many systems, it is not possible to visualize the phase space, since most of the interesting systems have more than three degrees of freedom. One interesting tool to ‘decrease the phase space dimensionality’ is the Poincaré section; it allows the visualization of the phase space information on two dimensions. Figure 9 exhibits a schema of

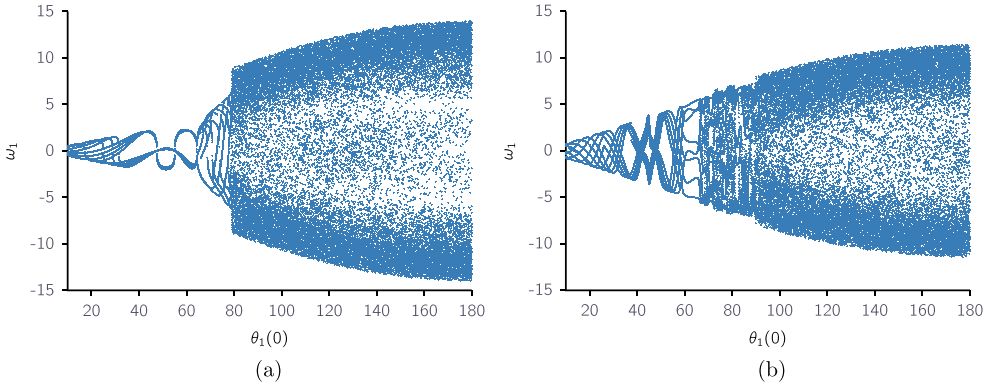


Figure 11. The double pendulum bifurcation diagrams show the chaos–order transition with two different initial conditions. It was built using fourth-order Adams–Bashforth with $\delta t = 10^4$. For a chosen $\theta_1(0)$ and $\theta_2(0)$ with $\omega_1(0) = \omega_2(0) = 0$, the system was iterated 10^5 times; then 8 points on the line $\omega_2(t) = 0$ on the $\omega_1(t) \times \omega_2(t)$ plane were obtained to compose the diagram. (a) Symmetric ($\theta_2(0) = \theta_1(0)$). (b) Asymmetric ($\theta_2(0) = 0$).

a Poincaré section and describes the process involved (Poincaré sections of the double pendulum can be found in [2]). The Poincaré section gives a distribution of points on two dimensions; a spatial disordered pattern is an indication of a chaotic motion, and a regular pattern is an indication of a quasiperiodic motion.

Even by choosing only two variables of the phase space, to build a phase plane, it is possible to have a reasonable intuition of what is happening on the complete phase space. Figure 10 shows two variables of the pendulum trajectory for two different initial conditions. On the left, we observe a regular pattern formed by a quasiperiodic orbit. On the other side, the right exhibits an irregular pattern, characteristic of a chaotic motion. One can use this fact to build a bifurcation diagram, a useful tool to visualize the route to chaos. For our purpose here, a bifurcation diagram is then built through the relation with the dynamics of a carefully chosen quantity that should reflect chaotic or periodic behavior versus some parameter of the system. Actually, there is a whole field dedicated to the analysis of bifurcation in dynamical systems called the ‘bifurcation theory’ [28].

Records of the position where trajectories cross a single line on the phase plane can reflect the regularity, or disorder, of the whole 2D pattern. Those records for different control parameters can be used to build a bifurcation diagram. It is not difficult to understand why the records on a single line can reflect the transition from order to chaos. On a quasiperiodic motion, trajectories will cross the line approximately at the same points, since the system eventually returns close to its previous state. However, when the system is chaotic, the cross points will never be the same, since nearby orbits diverge from each other. However, because the trajectories are restricted to a region of the phase space, they will ultimately come close again, but never on the exactly same point, leading to different abscissa crosses.

For the double pendulum, it is convenient to choose ω_1 and ω_2 for the phase plane, since those variables oscillate around zero. In this way it is easier to choose a Poincaré section that is frequently crossed by the system trajectory, a necessary condition to build a bifurcation diagram.

In figure 8(b), the Lyapunov exponent shows that there is a critical angle for which the pendulum is chaotic; here, with the bifurcation diagrams, it is possible to observe the same. In

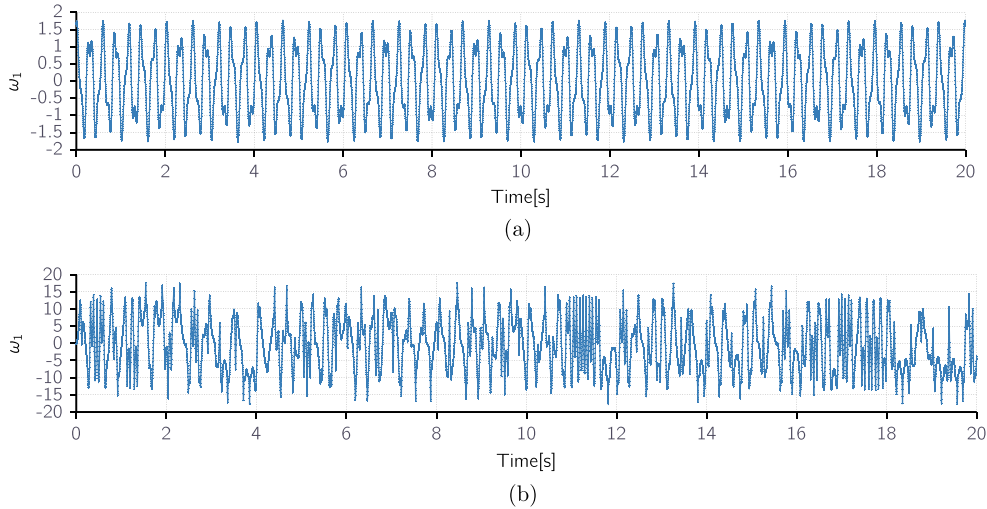


Figure 12. Examples of quasiperiodic and chaotic time series of the double pendulum. (a) Quasiperiodic time series, $\theta_1(0) = \theta_2(0) = 20^\circ$. (b) A chaotic time series, $\theta_1(0) = \theta_2(0) = 130^\circ$.

figure 11 the transition from a stable behaviour, with quasiperiodic orbits, to a chaotic one is depicted by a bifurcation diagram.

On the quasiperiodic regime, with a slight difference in initial conditions, there is just a slight difference between the points records on the Poincaré sections of the phase planes. That is why we can see continuous lines on the bifurcation diagram where the dynamics are quasiperiodic. However, for the chaotic behaviour, a slight difference in the initial conditions leads to very different points records on the Poincaré sections of the phase planes. This leads to a very irregular pattern on the bifurcation diagram for the chaotic behaviour.

As opposed to the Lyapunov exponent, bifurcation diagrams give just a qualitative information about the system transition from quasiperiodic behaviour to a chaotic one; nevertheless, it is intuitive and more easy to calculate.

A similar analysis of the bifurcations on the double pendulum can be found in [2], and a more extensive analysis on a similar model, a forced double pendulum with linear springs on the joints, can also be found in [1].

4.3. Time series

In this section we will try to predict the system behaviour using just one dimension, that is, a time series S of one variable of the system, a sequence of points typically measured at uniform time intervals. A common notation is:

$$S = \{s_1, s_2, s_3, \dots, s_n, \dots, s_N\} \quad (13)$$

where s_i are the successive measures of the quantity of interest. Time series analysis is important; it is frequently the only available information about the dynamics of an experiment.

When obtaining a time series, one should make sure to take in a time interval that includes many characteristic periods. There is no easy recipe when dealing with an aperiodic system; the interval should be as large as possible to check if the system is in an aperiodic

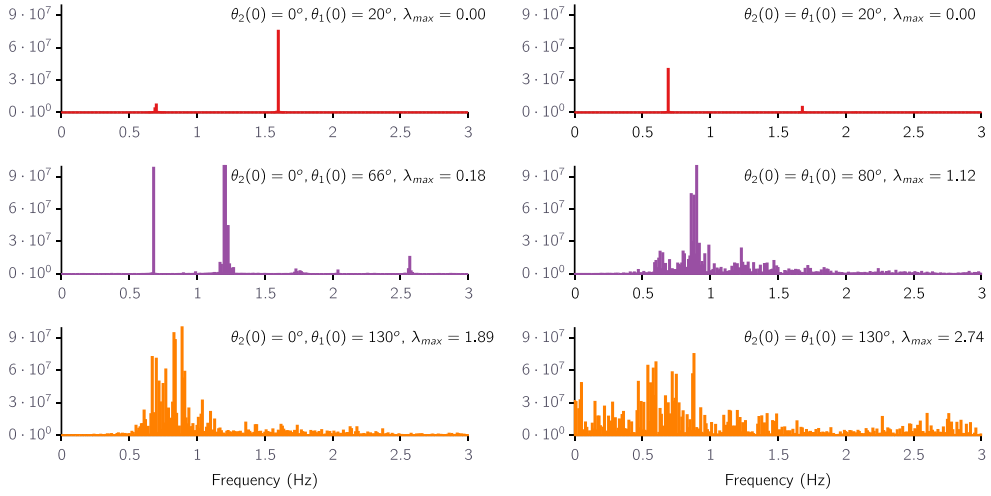


Figure 13. Power spectrum for many different initial conditions. Note that for a large Lyapunov exponent there are many frequencies.

state or in a transient one. Here, we have used the same parameters of the previous analysis; however, we sampled the numerical integration at every 200 steps and used 10000 points after discarding the first 100000 steps. In figure 12 there are examples of a regular time series and a chaotic one.

4.3.1. Fourier transform. The Fourier transform is probably the most common method of time series analysis, having applications in many fields, like biology [29, 30], noise reduction [31, 32], image processing [33, 34] and many others.

The Fourier transform is based on the fact that a function can be represented as the sum of other oscillatory functions, given that some conditions are fulfilled. From this it is possible to find $c(k)$, a coefficient that provides the relevance of each frequency k .

In applications, a *fast Fourier transform* algorithm (FFT) is used to compute faster the Fourier transforms of discrete data. The most common FFT algorithm is the Cooley–Tukey algorithm [35], although there are some alternatives [36–39].

Figure 13 is the power spectrum $|c(k)|^2$ of the ω_1 time series for different initial conditions. A chaotic behaviour, as was previously shown, does not have a characteristic period or frequency. The cases $(\theta_1(0) = \theta_2(0) = 20)$ and $(\theta_1(0) = 0, \theta_2(0) = 20)$ present few frequencies, as is expected for a quasiperiodic behaviour. For $(\theta_1(0) = \theta_2(0) = 130)$ and $(\theta_1(0) = 0, \theta_2(0) = 130)$ the graphic shows many frequencies, a sign of chaotic behaviour. However, for other angles with a small Lyapunov exponent, it is difficult to determine precisely if the system is in a chaotic state or not, hindering the analyses.

Another matter is a random time series; it has no characteristic frequency, similar to chaotic time series. So, we must be careful not to confuse chaos and noise when using Fourier analysis. Another limitation in practical situations is that the Fourier transform is not well defined for nonstationary signals.

Although the Fourier analysis has been very useful for linear systems, by being a simple and fast method, there are needs for other methods, e.g., nonlinear methods, for the analysis

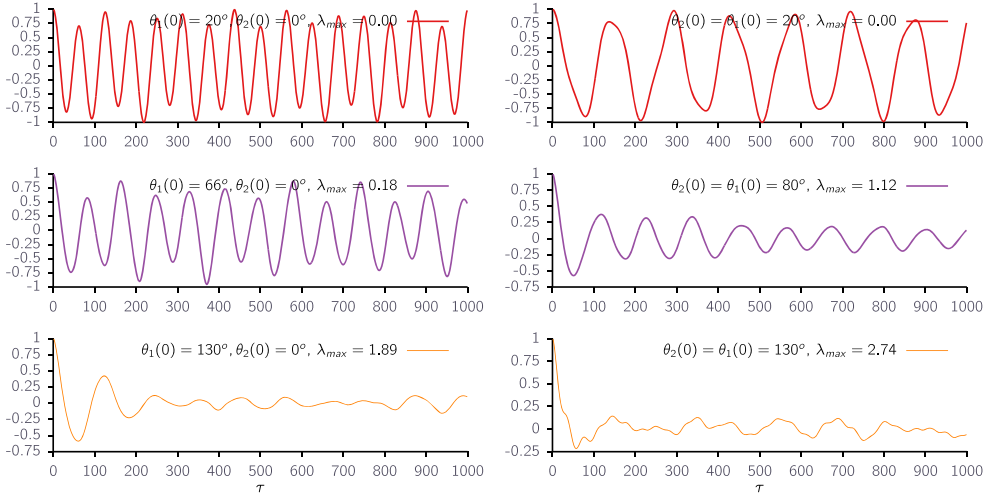


Figure 14. Autocorrelation of $\omega_1(t)$ for many different initial conditions. Note how the autocorrelation vanishes for large Lyapunov exponents.

of time series of chaotic systems. Still, it can be used for qualitative analysis since it is of easy and efficient implementation.

4.3.2. Autocorrelation function. Autocorrelation measures if two points separated by a distance τ are *linearly correlated*. It is defined as

$$C_L(\tau) = \frac{\frac{1}{N} \sum_{m=1}^N [s_{(m+\tau)} - \bar{s}][s_m - \bar{s}]}{\sigma_s^2}, \quad (14)$$

where \bar{s} is the mean of the time series. $C_L \in [-1, 1]$ and when $C_L \rightarrow 1$ is an indication of *correlation*, $C_L \rightarrow -1$ of *anti-correlation*, and when $C_L \rightarrow 0$ is an indication of no *correlation*.

For a periodic series, the autocorrelation function will also show periodicity. For a chaotic time series, neighboring points in the phase space get exponentially far from each other, leading to no correlation after a finite time; consequently, the autocorrelation function should vanish after some time.

In figure 14 it is possible to observe the autocorrelation function of $\omega_1(t)$ for different initial conditions. Once again, we choose to work with the angular velocity because its values oscillate around zero. The results presented in figure 14 are similar to the ones present in figure 13, where chaos cannot be detected for small Lyapunov exponents. Nevertheless, the first zero of the autocorrelation function indicates how long it takes an event to lose *correlation* with past events, and this is important for other purposes [12].

This method, like the Fourier analysis, can only describe qualitatively the transition to chaos.

4.3.3. Recurrence plots. The recurrence plot is a very interesting method developed to help the visualization of the recurrences on the phase space [40]. As we have commented before, many physical systems have more than three degrees of freedom; therefore, the visualization of the phase space becomes difficult. The plot is generated from a square matrix $M \times M$,

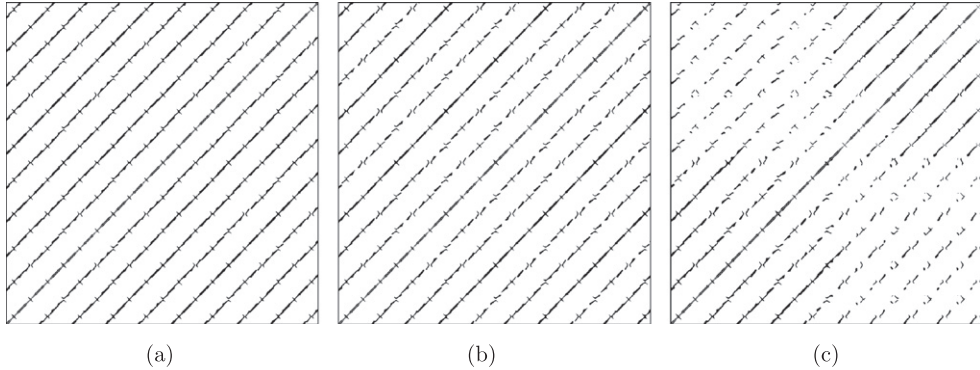


Figure 15. Recurrence plots of different initial conditions. (a) Periodic state ($\theta_1(0) = \theta_2(0) = 78^\circ$). (b) Transition state ($\theta_1(0) = \theta_2(0) = 79.14^\circ$). (c) Chaotic state ($\theta_1(0) = \theta_2(0) = 80^\circ$).

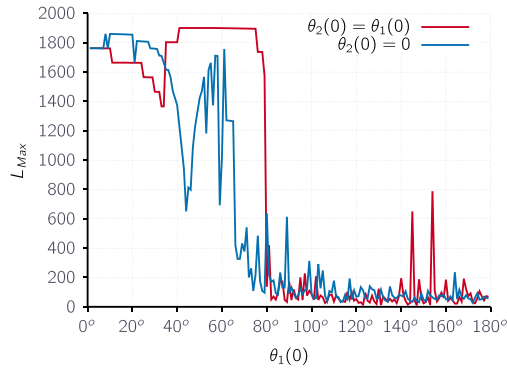


Figure 16. Graphic showing the chaos-order transition through the RQA method.

where the elements (i, j) are painted one color in the case where the vector $\vec{x}(i)$ and $\vec{x}(j)$ are closer than a distance ϵ on the phase space; otherwise, the point is painted another color. This can be summarized as:

$$R(i, j) = \Theta(\epsilon - \|\vec{x}(i) - \vec{x}(j)\|), \quad \vec{x}(i) \in \mathbb{R}^N, \quad i, j = 1, \dots, M \quad (15)$$

where Θ is the Heaviside step function and $\|\cdot\|$ is a norm, e.g., euclidean norm.

The method depends on the choice of the ϵ parameter. Although there are some recipes/instructions on how to choose this parameter in the literature [41, 42], in this study we use $\epsilon = 0.4\sigma$, where σ is the standard deviation of the distance between the points on the phase space [43]. On the other hand, a clear advantage is that it analyses the phase space as a whole and not only one coordinate as in the case of the Fourier transform or the autocorrelation function. For the cases where only a time series is available, one can try to reconstruct the phase space from it using time-delay coordinates [44] (see [12] for more details).

Each type of structure in recurrence plots shows the indication of one kind of dynamic behaviour. Particularly, the diagonal lines are associated with periodicity, indicating that the system tends to visit frequently the same region of the phase space. When chaos starts to appear, the diagonal lines start to diminish.

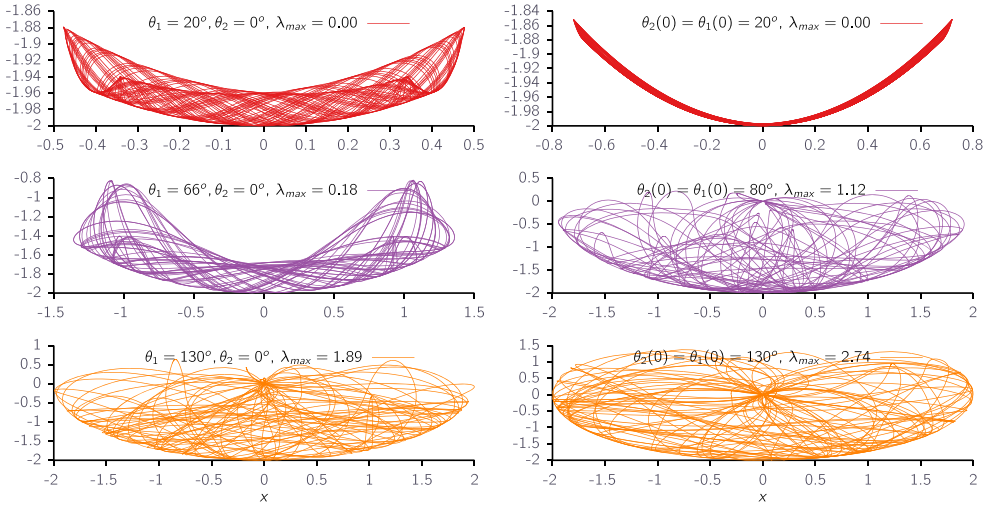


Figure 17. Position of the second mass, m_2 , where the abscissa is $x = l_1 \sin(\theta_1(t)) + l_2 \sin(\theta_1(t))$ and the ordinate is $y = -l_1 \cos(\theta_1(t)) - l_2 \cos(\theta_1(t))$. The position of m_1 has not been plotted because it is always a semicircle.

Figure 15 shows the recurrence plot for different initial conditions of the double pendulum; it is clear that it elucidates different behaviours. In figure 15(a), the periodic state shows a regular behaviour with very long diagonal lines, while figure 15(c) shows a very erratic pattern and figure 15(b) shows a state that is a transition between the others.

Although the recurrence plot was originally just a qualitative tool, it has developed the method known as recurrence quantitative analysis, or RQA [45], that quantifies the structures on the recurrence plots, helping to identify a specific kind of dynamics [41]. One of them is L_{\max} , the maximum diagonal line length. This quantity is related to the Lyapunov exponent of the system, since chaotic systems tend to have smaller diagonal lines on the recurrence plots. In figure 16 is possible to see that L_{\max} is able to predict the system transition to chaos, in good agreement with figure 8(b).

This method is very popular [46] and had been used to analyse different systems, like financial market [47], biology [43], molecular dynamics [48] and others. Possibly the most interesting feature of the recurrence plot is that it works even for short time series.

4.4. m_2 Trajectory

Some of the analysis of the previous sections are in the frequencies space, others in the phase space. However, it is not clear what is happening in the real world. Thus, it is important to investigate the trajectory of the second mass of the pendulum, m_2 , for different initial conditions, as seen in figure 17.

The quasiperiodic and chaotic motion shown in figures 8(b) and 13 can also be seen in the trajectory of the second mass, m_2 , in figure 17.

It is remarkable that the quasiperiodic state, at least for the asymmetric case, $\theta_1(0) = \{0, \pi\}, \theta_2(0) = 0$, where the trajectories are not squeezed, resembles a diffeomorphism of a

Lissajous curve. This is indication that the dynamics for low energies are similar to the ones of coupled harmonic oscillators.

It is important to note that when the pendulum is chaotic and has a large enough Lyapunov exponent, the behaviour of the trajectory is very erratic. Thus, the strange trajectory of a real double pendulum is the result of chaos.

5. Conclusion

We have studied the double pendulum, a classical problem in mechanics. We have discussed how the numerical results depend on the integration method. After we had made sure that the numerical integration is performing well, we were ready to understand more about the system dynamics. We found that the Lyapunov exponent and the bifurcation diagram methods can predict the transition of the pendulum behaviour, from a simple quasiperiodic behaviour to a chaotic one; while the former method is quantitative and is difficult to implement, the latter is qualitative and can be easily obtained. It was also shown that a Fourier analysis is not appropriate for the quantification of the order–chaos transition, since it only provides a qualitative hint of a change on the dynamics. The autocorrelation method is also qualitative; however, the interpretation is clearer. When dealing with the possibility of chaos, it is evident of the need of a better method to investigate time series. To improve the analysis of nonlinear systems, many nonlinear methods, used to analyse time series, have been developed. In this line was presented the recurrence plots, a simple method, yet very useful to understand the dynamics of the system, both qualitative and quantitative.

And finally, in section 4.4, a connection between what is happening in the phase space and the observed trajectory of the double pendulum was made.

As we have shown, even a simple system like a double pendulum can exhibit chaos, so it is imperative to understand how to apply nonlinear methods in such systems before trying them in much more complex ones, such as, time series of the human heartbeat [49], finance time series or other contemporary problems.

References

- [1] Yu P and Bi Q 1998 Analysis of non-linear dynamics and bifurcations of a double pendulum *J. Sound Vib.* **217** 691–736
- [2] Stachowiak T and Okada T 2006 A numerical analysis of chaos in the double pendulum *Chaos, Solitons & Fractals* **29** 417–22
- [3] Rafat M Z, Wheatland M S and Bedding T R 2009 Dynamics of a double pendulum with distributed mass *Am. J. Phys.* **77** 216–23
- [4] Levien R B and Tan S M 1993 Double pendulum: an experiment in chaos *Am. J. Phys.* **61** 1038–44
- [5] Vesely F J 2013 Of pendulums, polymers, and robots: computational mechanics with constraints *Am. J. Phys.* **81** 537–44
- [6] Anderson P W *et al* 1972 More is different *Science* **177** 393
- [7] Betzler N, Monk S, Wallace E, Otto S R and Shan G 2008 From the double pendulum model to full-body simulation: evolution of golf swing modeling *Sports Technol.* **1** 175–88
- [8] Rubí J, Rubio A and Avello A 2002 Swing-up control problem for a self-erecting double inverted pendulum *Control Theory and Applications, IEEE Proc.* **149** 169–75
- [9] Yamakita M, Iwashiro M, Sugahara Y and Furuta K 1995 Robust swing up control of double pendulum *Proc. American Control Conf.* vol 1 pp 290–5
- [10] Graichen K, Treuer M and Zeitz M 2007 Swing-up of the double pendulum on a cart by feedforward and feedback control with experimental validation *Automatica* **43** 63–71

- [11] Hoover W G, Hoover C G and Posch H A 1990 Lyapunov instability of pendulums, chains, and strings *Phys. Rev. A* **41** 2999–3004
- [12] Abarbanel H D I, Browz R, Sidorowich J J and Tsimring L S 1993 The analysis of observed chaotic data in physical systems *Rev. Mod. Phys.* **65** 1331–92
- [13] Goldstein H 1981 *Classical Mechanics* (Reading, MA: Addison-Wesley)
- [14] Boyce W E and DiPrima R C 2001 *Elementary Differential Equations* 7th edn (New York: Wiley)
- [15] Faires J D and Burden R L 2003 *Numerical Analysis* 1st edn (USA Thomson)
- [16] Iserles A 2009 *A First Course in the Numerical Analysis of Differential Equations* vol 44 (New York: Cambridge University Press)
- [17] Donnelly D and Rogers E 2005 Symplectic integrators: an introduction *Am. J. Phys.* **73** 938–45
- [18] Blanes S and Iserles A 2012 Explicit adaptive symplectic integrators for solving Hamiltonian systems *Celest. Mech. Dyn. Astron.* **114** 297–317
- [19] Channell P J and Scovel C 1990 Symplectic integration of Hamiltonian systems *Nonlinearity* **3** 231
- [20] Yoshida H 1993 Recent progress in the theory and application of symplectic integrators *Qualitative and Quantitative Behaviour of Planetary Systems* (Dordrecht: Springer) 27–43
- [21] Sanz-Serna J M and Calvo M P 1994 *Numerical Hamiltonian Problems* 1st edn (London: Chapman & Hall)
- [22] Stuchi T J 2002 Symplectic integrators revisited *Braz. J. Phys.* **32** 958–79
- [23] Benettin G, Galgani L, Giorgilli A and Strelcyn J-M 1980 Lyapunov characteristic exponents for smooth dynamical systems and for Hamiltonian systems; a method for computing all of them: 1. Theory *Meccanica* **15** 9–20
- [24] Wolf A, Swift J B, Swinney H L and Vastano J A 1985 Determining Lyapunov exponents from a time series *Physica D Nonlinear Phenomena* **16** 285–317
- [25] Earnshaw J C and Haughey D 1993 Lyapunov exponents for pedestrians *Am. J. Phys.* **61** 401–7
- [26] Tobochnik J and Gould H 1989 Quantifying chaos *Comput. Phys.* **3** 86
- [27] Shinbrot T, Grebogi C, Wisdom J and Yorke J A 1992 Chaos in a double pendulum *Am. J. Phys.* **60** 491–9
- [28] Kuznetsov Y 2004 *Elements of Applied Bifurcation Theory* (New York: Springer)
- [29] Aharoni A, Ric de Vos C H, Verhoeven H A, Maliepaard C A, Kruppa G, Bino R and Goodenowe D B 2002 Nontargeted metabolome analysis by use of Fourier transform ion cyclotron mass spectrometry *Omics: J. Integrat. Biol.* **6** 217–34
- [30] Yoganathan A P, Gupta R, Udwadia F E, Miller J W, Corcoran W H, Sarma R, Johnson J L and Bing R J 1976 Use of the fast Fourier transform for frequency analysis of the first heart sound in normal man *Med. Biol. Eng.* **14** 69–73
- [31] Boll S 1979 Suppression of acoustic noise in speech using spectral subtraction *Acoustics, Speech and Signal Processing, IEEE Trans.* **27** 113–20
- [32] Soon I Y, Koh S N and Yeo C K 1998 Noisy speech enhancement using discrete cosine transform *Speech Commun.* **24** 249–57
- [33] Lim J S 1990 *Two-Dimensional Signal and Image Processing* (Englewood Cliffs, NJ: Prentice Hall) 710 pp
- [34] Schalkoff R J 1989 *Digital Image Processing and Computer Vision* (New York: Wiley)
- [35] Cooley J W and Tukey J W 1965 An algorithm for the machine calculation of complex fourier series *Math. Comput.* **19** 297–301
- [36] Murakami H 1966 Real-valued fast discrete fourier transform and cyclic convolution algorithms of highly composite even length *Proc. IEEE Int. Conf. on Acoustics, Speech and Signal Processing, ICASSP-96* vol 3 pp 1311–4
- [37] Good I J 1958 The interaction algorithm and practical fourier analysis *J. R. Stat. Soc. B (Methodological)* 361–72
- [38] Rader C M 1968 Discrete fourier transforms when the number of data samples is prime *Proc. IEEE* **56** 1107–8
- [39] Bluestein L 1970 A linear filtering approach to the computation of discrete fourier transform *Audio and Electroacoustics, IEEE Trans.* **18** 451–5
- [40] Eckmann J-P, Oliffson Kamphorst S and Ruelle D 1987 Recurrence plots of dynamical systems *Europhy. Lett.* **4** 973
- [41] Marwan N, Romano M C, Thiel M and Kurths J 2007 Recurrence plots for the analysis of complex systems *Phys. Rep.* **438** 237–329

- [42] Schinkel S, Dimigen O and Marwan N 2008 Selection of recurrence threshold for signal detection *Eur. Phys. J. Special Topics* **164** 45–53
- [43] Marwan N, Wessel N, Meyerfeldt U, Schirdewan A and Kurths J 2002 Recurrence-plot-based measures of complexity and their application to heart-rate-variability data *Phys. Rev. E* **66** 026702
- [44] Packard N H, Crutchfield J P, Farmer J D and Shaw R S 1980 Geometry from a time series *Phys. Rev. Lett.* **45** 712–6
- [45] Webber C L Jr, Marwan N, Facchini A and Giuliani A 2009 Simpler methods do it better: success of recurrence quantification analysis as a general purpose data analysis tool *Phys. Lett. A* **373** 3753–6
- [46] Marwan N 2008 A historical review of recurrence plots *Eur. Phys. J. Special Topics* **164** 3–12
- [47] Fabretti A and Ausloos M 2005 Recurrence plot and recurrence quantification analysis techniques for detecting a critical regime *Int. J. Mod. Phys. C* **16** 671–706
- [48] Giuliani A and Manetti C 1996 Hidden peculiarities in the potential energy time series of a tripeptide highlighted by a recurrence plot analysis: a molecular dynamics simulation *Phys. Rev. E* **53** 6336–40
- [49] Galhardo C E C, Penna T J P, de Menezes M A and Soares P P S 2009 Detrended fluctuation analysis of a systolic blood pressure control loop *New J. Phys.* **11** 103005